



Article

# Linear Polarization Signatures of Particle Acceleration in High-Synchrotron-Peak Blazars

Alan P. Marscher 1,\* and Svetlana G. Jorstad 1,2 a

- <sup>1</sup> Institute for Astrophysical Research, Boston University, Boston, MA 02215, USA
- Astronomical Institute, St. Petersburg State University, Universitetsky Prospekt, 28, Petrodvorets, 198504 St. Petersburg, Russia
- \* Correspondence: marscher@bu.edu

**Abstract:** Blazars whose synchrotron spectral energy distribution (SED) peaks at X-ray energies need to accelerate electrons to energies in the >100 GeV range in relativistic plasma jets at distances of parsecs from the central engine. Compton scattering by the same electrons can explain high luminosities at very high photon energies (>100 GeV) from the same objects. Turbulence combined with a standing conical shock can accomplish this. Such a scenario can also qualitatively explain the level and variability of linear polarization observed at optical frequencies in these objects. Multi-wavelength polarization measurements, including those at X-ray energies by *the Imaging X-ray Polarimetry Explorer (IXPE)*, find that the degree of polarization is several times higher at X-ray than at optical wavelengths, in general agreement with the turbulence-plus-shock picture. Some detailed properties of the observed polarization can be naturally explained by this scenario, while others pose challenges that may require modifications to the model.

Keywords: galaxies: active; galaxies: jets; quasars: general; BL Lacertae objects: general



Citation: Marscher, A.P.; Jorstad, S.G. Linear Polarization Signatures of Particle Acceleration in High-Synchrotron-Peak Blazars. *Universe* 2022, 8, 644. https:// doi.org/10.3390/universe8120644

Academic Editors: Ioana Dutan and Nicholas R. MacDonald

Received: 8 November 2022 Accepted: 30 November 2022 Published: 4 December 2022

**Publisher's Note:** MDPI stays neutral with regard to jurisdictional claims in published maps and institutional affiliations.



Copyright: © 2022 by the authors. Licensee MDPI, Basel, Switzerland. This article is an open access article distributed under the terms and conditions of the Creative Commons Attribution (CC BY) license (https://creativecommons.org/licenses/by/4.0/).

## 1. Introduction

Blazars are active galactic nuclei whose emission across the electromagnetic spectrum is almost completely dominated by nonthermal radiation from high-energy plasma flowing in a jet that is propelled toward the line of sight at near-light speeds. The radiation results from ultra-high-energy particles interacting with magnetic fields and photons, and is highly beamed toward us owing to the bulk relativistic flow velocity of the plasma. This radiation is linearly polarized at levels ranging from nearly zero to tens of percent at millimeter to optical wavelengths. Both the degree P and electric-vector position angle  $\chi$  of linear polarization (LP) are highly variable, although in some blazars the latter fluctuates about the jet direction [1,2]. This behavior has led to the proposal [3] that the plasma contains both turbulent and ordered components, with the latter corresponding, for example, to a helical magnetic field [4,5] or compression by a shock [6].

The spectral energy distribution (SED; see Figure 1 for a sketch) of a blazar consists of two major nonthermal components, one of which peaks at infrared to X-ray frequencies and is usually ascribed to synchrotron radiation. The luminosity of the other component reaches a maximum in the  $\gamma$ -ray range, resulting from processes that may be object-dependent. Here, we adopt the working hypothesis that Compton scattering by relativistic electrons in the jet is the dominant mechanism for the high-energy component of the SED. In blazars whose synchrotron component peaks at X-ray frequencies, termed "high synchrotron-peak" (HSP) sources, the high-energy SED component peaks at very high  $\gamma$ -ray energies (VHE,  $\geq$ 0.1 TeV). This requires efficient acceleration of electrons up to the VHE range.

In this work, we relate particle acceleration to the linear polarization properties in HSP blazars. We then adopt a model for blazar jets that includes shocks and turbulence. We present multi-wavelength polarization data that provide tests of theoretical scenarios for how the radiating particles—electrons in the model—attain energies up to TeV levels.

Universe 2022, 8, 644 2 of 10

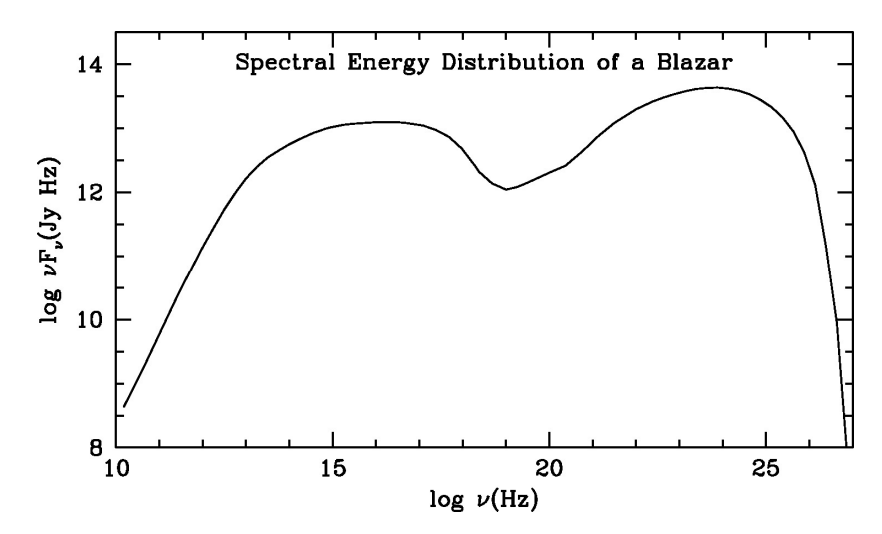


**Figure 1.** Sketch of the spectral energy distribution of a blazar. There are two peaks, one at low (infrared for low-synchrotron-peak blazars to X-ray for HSP BL Lac objects, the latter of which is shown here) and another at high ( $\gamma$ -ray) photon energies.

#### 2. Particle Acceleration Mechanisms in Blazars

Figure 2 sketches the model of a blazar jet that we adopt to interpret multi-wavelength observations of blazars. The inner jet region is threaded by a helical magnetic field that propagates down the jet along with the plasma [7]. The magnetic energy is converted to kinetic energy of the plasma in this region until equipartition is reached between the two. Beyond this point, the plasma becomes turbulent [3]. The jet over-expands such that its pressure becomes less than that of the external medium, which causes a conical recollimation shock to form [8]. (Others can form farther downstream as well [9].) We associate this standing shock with the "core," the compact, intense emission feature observed near the upstream end of millimeter-wave very long baseline interferometry images of blazar jets [10]. Surges in energy and/or higher velocities of the plasma injected into the base of the jet create moving shocks that are observed as bright knots with superluminal apparent velocities [11].

The process(es) by which electrons in the jet attain energies at VHE levels are highly debated. Diffusive shock acceleration, in which particles can cross the shock front many times, tends to be very efficient in non-relativistic shocks, such as those in supernova remnants [12]. The process is less effective at producing VHE particles if the plasma is magnetically dominated (as is likely the case in the most upstream regions of the jet), since this condition only allows weak shocks to form [13]. In addition, if the shocks are highly relativistic, electrons advect away from the shock before being able to cross the front multiple times, and hence only gain a modest boost in energy [13]. The latter problem is less severe if the shocks are oblique to the jet flow, as is the case for standing ("recollimation") shocks [14]. It can also be mitigated if the magnetic field is nearly parallel to the shock normal in the rest frame of the plasma that is crossing the shock front [14]. Magnetic reconnection, which occurs when two regions of plasma with oppositely directed magnetic fields come into contact, is another mechanism capable of accelerating electrons to the VHE range, e.g., [15]. It is most efficient in magnetically dominated plasmas. Turbulent magnetic fields can also energize electrons through second-order Fermi acceleration [16]. Magnetic fields that are sheared by cross-jet velocity gradients can also accelerate particles [17]. All of the above mechanisms are likely to operate in the relativistic jets of blazars at some level. A major question, however, is whether individual particle acceleration processes, or a combination of processes, are responsible for the most extreme behavior observed. Such behavior includes strong VHE emission, major flares, intra-day variability, and high, variable linear polarization.

Universe 2022, 8, 644 3 of 10

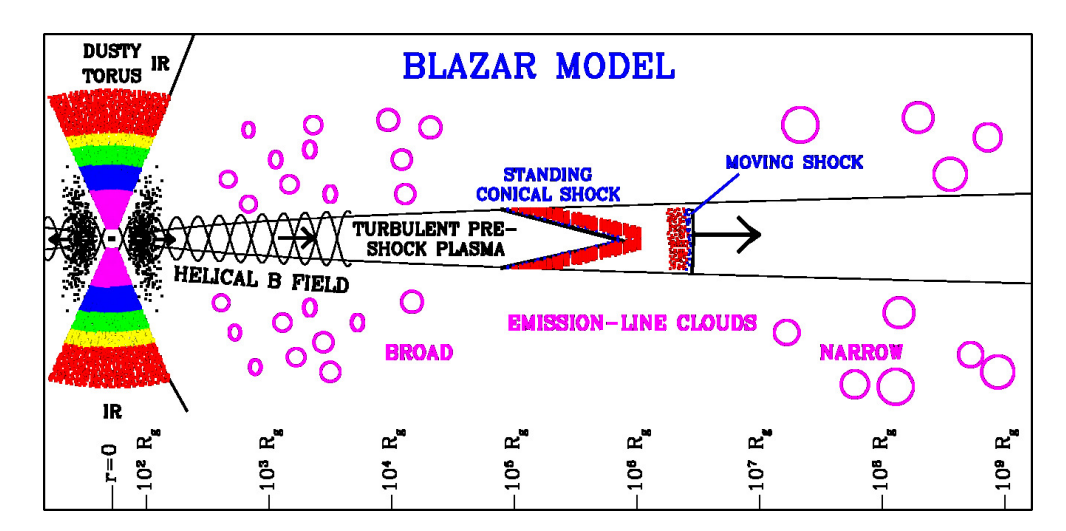


**Figure 2.** Sketch of the blazar model considered here. The linear scale is logarithmic (in units of the gravitational radius  $R_{\rm g}$ ) in order to fit all features into a single frame. The central engine on the left consists of a super-massive black hole surrounded in the equatorial region by an accretion disk whose temperature decreases outward, beyond which there is a hot ( $\sim$ 1200–1500 K), dusty molecular torus. Other features are marked. The thin blue regions next to the shock fronts represent the location of X-ray synchrotron emission, while the adjacent red regions correspond to lower-frequency (optical-IR) emission. The irregularities in the X-ray (blue) regions signify that only some turbulent cells have electrons of sufficiently high energies to emit synchrotron radiation at X-ray frequencies.

Polarization observations have the potential to discern among the different particle acceleration scenarios. Shocks partially align the magnetic field parallel to the shock front (transverse to the shock normal), leading to polarization along the jet direction, unless the shock is oblique to the jet. (A conical shock, however, still causes the polarization electric vector to align with the jet for most viewing directions [18,19].) Particle acceleration by sheared magnetic fields should be distinguished by polarization electric vectors that are oriented perpendicular to the jet. Turbulence—which can accelerate particles through both multiple, relatively minor magnetic-reconnection events and the second-order Fermi mechanism—is characterized by low polarization (mean <10%), with highly variable degree (standard deviation ~50% of the mean value) and position angle. Prominent flares caused by either major magnetic reconnection events or turbulence tend to cause rotations of the polarization electric vector, which should usually be smoother in the reconnection case [3,20–22]. In addition, the mean optical and X-ray degree of polarization from reconnection should be similar [20,21]. A smooth rotation can also occur as an emission feature travels along a helical magnetic field (which propagates down the jet) upstream of the turbulent zone [23,24]. Yet another phenomenon can occur in a blazar jet: a kink instability that twists the jet flow, causing magnetic reconnections and quasiperiodic oscillations in both the flux and polarization [25,26], as has been observed in BL Lacertae [27].

#### 3. Observations

The authors and their collaborators observe several HSP BL Lac objects as part of a multi-waveband monitoring program of  $\gamma$ -ray bright blazars. The observations include optical flux and linear polarization measurements at Boston University's Perkins Telescope (operated by Lowell Observatory prior to 2018). The acquisition and analysis of the limited optical data presented here is detailed in [2], which also displays multi-year  $\gamma$ -ray, X-ray, and optical light curves, as well as optical linear polarization vs. time—including some inter- and intra-day variations—and 43 GHz images made with data from the Very Long Baseline Array (VLBA). When calculating the flux density and degree of polarization, the host galaxy starlight—which tends to be significant in HSP blazars—has been subtracted

Universe 2022, 8, 644 4 of 10

according to the prescription of [28]. Figure 3 presents flux and polarization vs. time plots for the two prominent HSP blazars Mkn421 and Mkn501, updated from those displayed in [2].

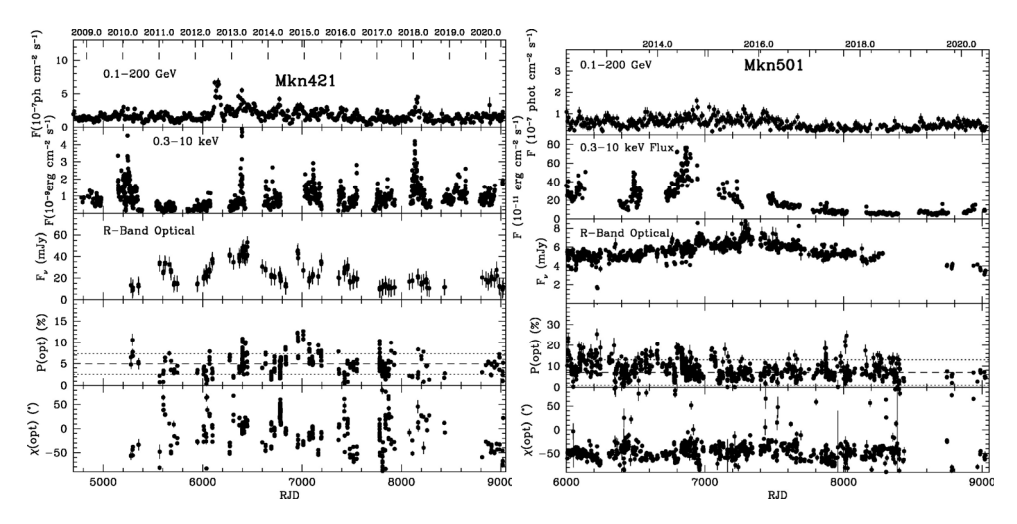


**Figure 3.** Multi-wavelength light curves and optical linear polarization vs. time for the two HSP blazars Mkn421 and Mkn501. RJD is the Julian date minus 2,450,000. The contribution of starlight from the host galaxy has been subtracted. In the optical polarization panel (4th from the top), the dashed line is the mean degree of polarization, while the dotted lines indicate  $\pm 1$  standard deviation from the mean. Updated from [2].

Recently, X-ray linear polarization measurements have been made possible by the Imaging X-ray Polarimetry Explorer (IXPE) mission [29]. IXPE detected polarization of both Mkn421 [30] and Mkn501 [31] over the energy range of 2–8 keV in 2022. In the case of Mkn501,  $P_{\rm X}=10\pm2\%$  and  $\chi_{\rm X}=134^{\circ}\pm5^{\circ}$  during one 2-day measurement and  $P_{\rm X}=11\pm2\%$  and  $\chi_{\rm X}=115^{\circ}\pm4^{\circ}$  during another 2-day pointing 18 days later. During the same epochs, the optical polarization was  $P_{\rm O}=4\pm1\%$  and  $\chi_{\rm O}=119^{\circ}\pm9^{\circ}$  and  $P_{\rm O}=5\pm1\%$  and  $P_{\rm O}=117^{\circ}\pm3^{\circ}$ —similar in position angle but a factor of 2–3 times lower than the X-ray degree of polarization. The IXPE measurements of Mkn421 give  $P_{\rm X}=15\pm2\%$  and  $P_{\rm X}=15\pm2\%$  an

# 4. Turbulence Plus Shock Model

Visual inspection of the bottom two panels of Figure 3 reveals similarities in the degree of optical polarization  $P_o$  of Mkn421 and Mkn501: it is highly variable in both objects. However, the temporal behavior of the electric-vector position angle  $\chi$  differs between them. While  $\chi_o$  in Mkn501 rarely deviates by more than 10° from the direction of the jet in 43 GHz VLBA images,  $120^\circ \pm 12^\circ$  (same as  $\chi = -60^\circ$  [32]), it varies across the full range of  $-90^\circ$  to  $+90^\circ$  in Mkn421, with only a modest "preference" for near-alignment with the jet direction of  $-14^\circ \pm 14^\circ$  [32]. The behavior of another prominent HSP blazar monitored by the authors, 1ES 1959 + 650, is similar to that of Mkn501 (see website [33]).

The combination of the strong variability of the optical polarization and the modest level of the degree of polarization—typically a few percent to ~20%, with only occasional higher values—can be explained if the magnetic field in the blazar emission region is at least partly disordered, as occurs in turbulent plasma. However, turbulence should result in random polarization position angles, while in a large fraction of blazars (e.g., Mkn501; see Figure 3, right)  $\chi_0$  varies about a "preferred" direction, which is usually roughly parallel to the jet, as seen in millimeter-wave VLBA images [2]. The mean magnetic field direction is therefore approximately perpendicular to the jet. As discussed in §2 above, this orientation can occur in a few different ways: a moving or standing shock, which partially orders

Universe 2022, 8, 644 5 of 10

the field, or, equivalently, an ordered helical field component on which the turbulent field is superposed. Magnetic reconnection would have a similar polarization direction if the helical field injected at the base of the jet were to switch handedness (from clockwise to counterclockwise or vice versa). Here, we consider the turbulence-plus-shock model, since it is capable of explaining the combination of order and disorder displayed by the behavior of the flux and polarization of blazars.

One of the primary radiative characteristics of shocks is frequency stratification [34]. The particles are accelerated in a thin layer at the shock front, then lose energy as they advect away from the shock. Since the frequency at which a particle emits the most is proportional to the energy squared, the highest frequencies can only be emitted very close to the shock front. Lower-frequency radiation can extend to greater distances from the shock front. This is illustrated for both the standing and moving shocks in Figure 2. The entire shocked region can radiate at frequencies below some value  $\nu_b$ , above which the spectral slope steepens by an additive factor of 0.5.

The thickness x of the region beyond the shock front where substantial emission occurs at frequency  $\nu$  depends on the radiative energy losses, which in turn depend on the magnetic field B and energy density of ambient photons (which serve as seed photons for Compton scattering)  $u_{\rm ph}$ , both measured in the rest frame of the emitting plasma:

$$x(\nu) \approx 4 \times 10^{-4} (B^2 + 8\pi u_{\rm ph})^{-1} [B\delta/\nu_{15}(1+z)]^{\frac{1}{2}},$$
 (1)

where  $v_{15}$  is the observed frequency in units of  $10^{15}$  Hz,  $\delta$  is the Doppler beaming factor, and z is the redshift of the host galaxy [34].

Under the assumption, adopted here, that the high-energy portion of the SED corresponds to Compton scattered emission, one can relate  $u_{ph}$  to B via the ratio of the high-energy to low-energy  $vF_v$  peaks:

$$u_{\rm ph} = \left(B^2 / 8\pi\right) \frac{(\nu F_{\nu})_{\rm high}}{(\nu F_{\nu})_{\rm low}} \tag{2}$$

Values of the magnetic field strength derived for the "core" and other very compact regions in blazars are commonly in the range of 0.02 to 3 G (e.g., [34–36]). Ratios of the SED peaks are typically 1–5 for HSP blazars and <1 to 1000 for low-synchrotron-peak (LSP) blazars, with the higher values occurring during major flares [37]. For an HSP in an average flux state, we adopt  $\delta$  = 20, B = 0.02 G, and an SED peak ratio = 1 to estimate  $x_x \approx 0.01$  pc at an X-ray energy of 4 keV and  $x_o \approx 0.5$  pc at the optical R band.

We propose a physical scenario similar to [3]. The jet, whose energy density is likely to be magnetically dominated upstream of the "core" [7,38–43], becomes unstable (e.g., to current-driven instabilities [44]) as the particle kinetic energy density reaches equipartition with the magnetic energy density. This generates turbulence in the ambient jet, with many magnetic reconnection events and second-order Fermi acceleration creating an ambient plasma containing a substantial population of relativistic particles (see above). The particles are further energized via diffusive shock acceleration when they encounter shock waves, and the electrons thus accelerated generate the bulk of the synchrotron and Compton-scattered emission observed from the blazar. The highest-energy, X-ray-emitting electrons thus produced only maintain their energies over a narrow region whose thickness is given by Equation (1). Optically emitting electrons can persist over a larger region, since  $x_{\rm opt} \gg x_{\rm x-ray}$  because of their weaker radiative losses.

The typical degree of optical polarization in Mkn421 and Mkn501 is 5–10%. This value, combined with the tendency—stronger for Mkn501—for  $\chi_0$  to be similar to the position angle of the jet, can be explained by compression of turbulent plasma by a shock [18,19]. For simplicity, let us assume that the ordered component remains constant, although computer simulations indicate that it may decay with distance from the shock front [45]. The magnetic field can then be approximated as N(x) turbulent cells—each with its own mag-

Universe 2022, 8, 644 6 of 10

netic field direction (see [3,46,47])—superposed on the ordered component  $B_{\rm ord}$ . The mean polarization is that of the ordered component, ~75% (the value for a typical optical spectral slope [46]) with position angle  $\chi_{\rm ord}$ , vector averaged with the sum of the polarization of the turbulent cells, ~  $0.75/\sqrt{N(x)}$ , where the latter has a random vector-averaged position angle  $\chi_{\rm turb}$ . The mean net normalized Stokes parameters are then

$$\langle q \rangle = 0.75 [f_{\text{ord}} \cos 2\chi_{\text{ord}} + (1 - f_{\text{ord}}) N^{-\frac{1}{2}}(\nu) \cos 2\langle \chi_{\text{turb}} \rangle]$$
 (3)

$$\langle u \rangle = 0.75 [f_{\text{ord}} \sin 2\chi_{\text{ord}} + (1 - f_{\text{ord}}) N^{-\frac{1}{2}}(\nu) \sin 2\langle \chi_{\text{turb}} \rangle]. \tag{4}$$

The mean degree of polarization is given by

$$\langle P \rangle^2 = \langle q \rangle^2 + \langle u \rangle^2 \approx 0.56 [f_{\text{ord}}^2 + (1 - f_{\text{ord}})^2 N^{-1}(\nu) +$$

$$2f_{\text{ord}}(1 - f_{\text{ord}})N^{-\frac{1}{2}}(\cos 2\chi_{\text{ord}}\cos 2\langle\chi_{\text{turb}}\rangle + \sin 2\chi_{\text{ord}}2\langle\chi_{\text{turb}}\rangle)]. \tag{5}$$

Given the randomness of  $\chi_{turb}$ , the term on the second line of Equation (5) averages to zero. The equation then reduces to

$$\langle P \rangle \approx \sqrt{\langle P \rangle^2} \approx 0.75 [f_{\text{ord}}^2 + (1 - f_{\text{ord}})^2 N^{-1}(\nu)]^{1/2}$$
 (6)

If the emission region is cylindrical, the number of turbulent cells  $N(\nu) \propto x(\nu) \propto \nu^{-1/2}$ . For an X-ray frequency of 9.6  $\times$  10<sup>17</sup> Hz (4 keV), compared with the optical R-band frequency of 4.6  $\times$  10<sup>14</sup> Hz, we find  $N_{\rm o} \approx 50~N_{\rm x}$ . For example, if 20 cells participate in the X-ray emission, so that  $N_{\rm x}$  = 20 and  $N_{\rm o} \approx 1000$ , and if  $f_{\rm ord}$  = 0.05, the model predicts that  $\langle P_{\rm x} \rangle \approx 16\%$  and  $\langle P_{\rm o} \rangle \approx 4\%$ . This factor of ~4 higher X-ray than optical polarization is similar to the results found for Mkn421 and Mkn501.

Based on numerical simulations [1], the measured value of  $\langle P \rangle$  should fluctuate about the mean with a standard deviation  $\sim 0.5 \langle P \rangle$ . If the dimension of a cell in the direction of the jet is much less than  $x(\nu)$ , this should occur on a time scale for a layer of turbulent cells to cross the emission region

$$t_{\rm cross} \approx \frac{x(\nu)}{c} \frac{(1+z)}{\delta} \sim 0.5 (B^2 + 8\pi u_{\rm ph})^{-1} \left[ \frac{B(1+z)}{\nu_{15} \delta} \right]^{\frac{1}{2}} {\rm days} \ (\nu \ge \nu_{\rm b}),$$
 (7)

measured in the observer's frame, where  $v_b$  is the frequency at which x(v) equals the full extent of the shocked region,  $x_{\text{shock}}$  [34]. [Here, we assume that the size of the turbulent cells—which physically corresponds to the size scale at which flow energy is dissipated [48]—is less than  $x(\nu)$ .] At frequencies above  $\nu_b$  there is therefore a time delay of variations in flux and polarization that is proportional to  $\nu^{-0.5}$ . Adopting, as before,  $\delta$  = 20, B = 0.02 G, and an SED peak ratio = 1, we estimate  $t_{\rm cross} \sim 0.6$  days for the 4 keV X-ray-emitting region and ~28 days at the optical R band. The former implies that IXPE should have detected variations in the X-ray polarization in both Mkn421 and Mkn501 during the first observations in 2022, contrary to the observations [30,31]. The expected optical variability time scale of ~4 weeks can be compared with the changes in optical polarization when the object was observed with adequate time coverage. Five such time intervals of monitoring of Mkn501 are displayed in Figure 4. Although there are periods when the degree of polarization x(v) varies over a much shorter time scale than ~4 weeks observed in both Mkn421 and Mkn501 [2], the typical time scale for substantial (more than a factor of ~2) variations is 2-4 weeks. The periods of more rapid variations may be related to intermittent intra-day optical variations seen in blazars [48]. Perhaps the sizes of the turbulent cells fluctuate over time, with variations in flux and polarization becoming more pronounced when the cell sizes match the value of  $x(\nu)$  at the frequency of observation.

Universe 2022, 8, 644 7 of 10

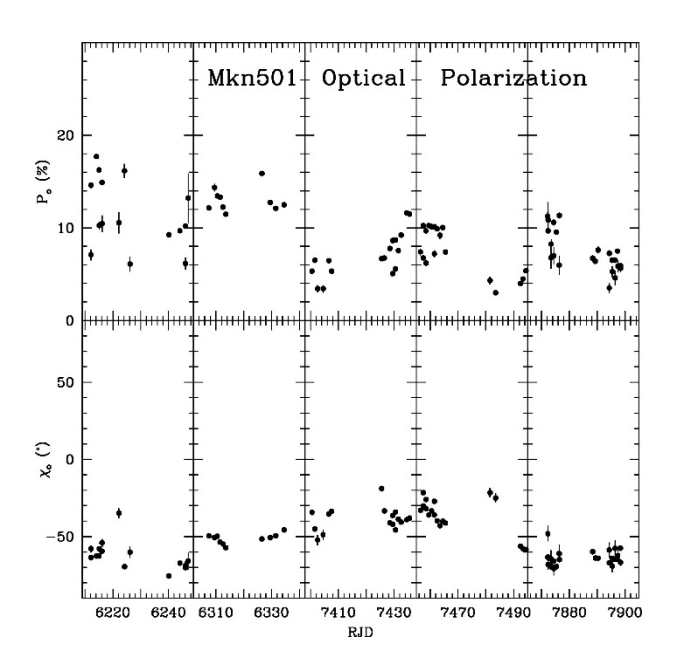


**Figure 4.** Optical polarization variability of Mkn501 during time intervals when the object was monitored with adequate time coverage. Data are from the data set displayed in Figure 3. The plotted points include data from Steward Observatory [49].

The stronger tendency of  $\chi$  to be similar to the position angle of the jet in Mkn501 than for Mkn421 requires that  $f_{\rm ord}$  (Mkn501) >  $f_{\rm ord}$  (Mkn421). The mean degree of optical polarization should be greater in Mkn501 as well. While this is consistent with Figure 3, the observed effect is small:  $\langle P_{\rm o} \rangle = 6.0\%$  in Mkn501 and  $\langle P_{\rm o} \rangle = 5.0\%$  in Mkn421.

The derivation of Equation (6) does not take into consideration the possibility that only some of the turbulent cells have magnetic field directions conducive to the acceleration of the highest-energy, X-ray-emitting electrons [2,3]. This would decrease the number of X-ray-emitting cells,  $N_x$ , and increase the ratio of  $\langle P_x \rangle / \langle P_o \rangle$ , allowing a larger value of  $f_{\rm ord}$  to explain the observed ratio. A decay in the ordered magnetic field component with distance from the shock [45] would decrease  $\langle P_o \rangle$ , and therefore also increase  $\langle P_x \rangle / \langle P_o \rangle$ .

The predicted degree of X-ray polarization corresponds to 100% synchrotron radiation. However, Compton scattering is expected to supply a fraction of the X-ray emission that increases with photon energy (see Figure 1). Since the degree of polarization of Compton scattering is expected to be no more than a few percent [50,51], the mean degree of polarization should decrease with photon energy. Measurement of this effect would serve as a test of Compton scattering as the main  $\gamma$ -ray emission mechanism. Modeling of the SED and energy-dependent polarization would also place a constraint on the minimum electron energy, since this parameter determines the ratio of Compton to synchrotron X-ray flux at a given photon energy.

### 5. Conclusions

The polarization properties of the HSP blazars Mkn421 and Mkn501 resemble those of the turbulence-plus-shock model. There are discrepancies: the observed time scales of optical polarization variability are sometimes shorter than predicted, while the X-ray polarization observed thus far remains nearly constant over longer time scales than expected. If the turbulence-plus-shock scenario is correct, future X-ray measurements will show much stronger variability on inter-day time scales.

The version of the model described in this work is simplified in order to allow analytic approximations to be derived that provide a sense of the properties of the polarization of HSP blazars. Computer simulations that include a more realistic rendering of turbulence, shocks, and particle acceleration, as well as more accurate calculations of time-dependent SEDs and multi-wavelength polarization, are needed to refine the estimates provided here

Universe 2022, 8, 644 8 of 10

and determine whether new behavior emerges as the model is developed in more detail. Such simulations are in progress.

**Author Contributions:** Conceptualization, A.P.M.; data curation, S.G.J.; formal analysis, S.G.J.; funding acquisition, A.P.M.; investigation, A.P.M.; writing—original draft, A.P.M.; writing—review and editing, S.G.J. All authors have read and agreed to the published version of the manuscript.

**Funding:** This research was funded in part by National Science Foundation grant AST-2108622 and NASA Fermi Guest Investigator grant 80NSSC22K1571.

**Institutional Review Board Statement:** Not applicable.

**Informed Consent Statement:** Not applicable.

**Data Availability Statement:** Data presented in Figure 3 are available upon request from the corresponding author.

Acknowledgments: The *Imaging X ray Polarimetry Explorer* (*IXPE*) is a joint US and Italian mission. The US contribution is supported by the National Aeronautics and Space Administration (NASA) and led and managed by its Marshall Space Flight Center (MSFC), with industry partner Ball Aerospace (contract NNM15AA18C). The Italian contribution is supported by the Italian Space Agency (Agenzia Spaziale Italiana, ASI) through contract ASI-OHBI-2017-12-I.0, agreements ASI-INAF-2017-12-H0 and ASI-INFN-2017.13-H0, and its Space Science Data Center (SSDC), and by the Istituto Nazionale di Astrofisica (INAF) and the Istituto Nazionale di Fisica Nucleare (INFN) in Italy. Optical data used in this work were obtained with the 1.8 m Perkins Telescope Observatory in Flagstaff, AZ, USA, which is owned and operated by Boston University. Data from the Steward Observatory spectropolarimetric monitoring project were used in this study. This program was supported by NASA Fermi Guest Investigator grants NNX08AW56G, NNX09AU10G, NNX12AO93G, and NNX15AU81G.

**Conflicts of Interest:** The authors declare no conflict of interest.

# References

- 1. Marscher, A.P.; Jorstad, S.G.; Williamson, K.E. Modeling the Time-Dependent Polarization of Blazars. *Galaxies* **2017**, *5*, 63. [CrossRef]
- 2. Marscher, A.P.; Jorstad, S.G. Frequency and Time Dependence of Linear Polarization in Turbulent Jets of Blazars. *Galaxies* **2021**, 9, 27. [CrossRef]
- 3. Marscher, A.P. Turbulent, Extreme Multi-Zone Model for Simulating Flux and Polarization Variability in Blazars. *Astrophys. J.* **2014**, 780, 87. [CrossRef]
- 4. Lyutikov, M.; Pariev, V.I.; Gabuzda, D.C. Polarization and Structure of Relativistic Parsec-scale ANG Jets. *Mon. Not. R. Astron. Soc.* **2005**, *360*, 869–891. [CrossRef]
- 5. Gabuzda, D.C. Evidence for Helical Magnetic Fields Associated with AGN Jets and the Action of a Cosmic Battery. *Galaxies* **2019**, 7, 5. [CrossRef]
- 6. Hughes, P.A.; Aller, H.D.; Aller, M.F. Polarized radio outbursts in BL Lacertae. I—Polarized emission from a compact jet. II—The flux, polarization of a piston-driven shock. *Astrophys. J.* **1985**, 298, 296–315. [CrossRef]
- 7. Vlahakis, N.; Königl, A. Magnetic Driving of Relativistic Outflows in Active Galactic Nuclei. 1. Interpretation of Parsec-Scale Accelerations. *Astrophys. J.* **2004**, *605*, *656*–*661*. [CrossRef]
- 8. Daly, R.A.; Marscher, A.P. The Gas Dynamics of Compact Relativistic Jets. *Astrophys. J.* 1988, 334, 552–559. [CrossRef]
- 9. Gómez, J.L.; Marti, J.M.; Marscher, A.P.; Ibañez, J.M.; Marcaide, J.M. Parsec-Scale Synchrotron Emission from Hydrodynamic Relativistic Jets in Active Galactic Nuclei. *Astrophys. J. Lett.* **1995**, 449, L19–L21. [CrossRef]
- 10. Marscher, A.P. The Core of a Blazar Jet. In *Extragalactic Jets Theory and Observation from Radio to Gamma Ray;* Rector, T.A., DeYoung, D.S., Eds.; Astronomical Society of the Pacific Conference Series: San Francisco, CA, USA, 2008; Volume 386, pp. 437–443.
- 11. Blandford, R.D.; Königl, A. Relativistic Jets in Compact Radio Sources. Astrophys. J. 1979, 232, 34–48. [CrossRef]
- 12. Bell, A.R.; Schure, K.M.; Reville, B.; Giacinti, G. Cosmic-Ray Acceleration and Escape from Supernova Remnants. *Mon. Not. R. Astron. Soc.* **2013**, *431*, *415–429*. [CrossRef]
- 13. Sironi, L.; Petropoulou, M.; Giannios, D. Relativistic Jets Shine through Shocks or Magnetic Reconnection? *Mon. Not. R. Astron. Soc.* **2015**, *450*, 183–191. [CrossRef]
- 14. Summerlin, E.J.; Baring, M.G. Diffusive Acceleration of Particles at Oblique, Relativistic, Magnetohydrodynamic Shocks. *Astrophys. J.* **2012**, 745, 63. [CrossRef]
- 15. Petropoulou, M.; Sironi, L. The Steady Growth of the High-Energy Spectral Cutoff in Relativistic Magnetic Reconnection. *Mon. Not. R. Astron. Soc.* **2015**, *481*, 5687–5701. [CrossRef]

Universe 2022, 8, 644 9 of 10

16. Stawarz, L.; Petrosian, V. On the Momentum Diffusion of Radiating Ultrarelativistic Electrons in a Turbulent Magnetic Field. *Astrophys. J.* **2008**, *681*, 1725–1744. [CrossRef]

- 17. Rieger, F.M.; Duffy, P. Particle Acceleration in Relativistic Shearing Flows: Energy Spectrum. Astrophys. J. 2022, 933, 149. [CrossRef]
- 18. Cawthorne, T.V. Polarization of Synchrotron Radiation from Conical Shock Waves. *Mon. Not. R. Astron. Soc.* **2006**, *367*, 851–859. [CrossRef]
- 19. Cawthorne, T.V.; Jorstad, S.G.; Marscher, A.P. Evidence for Recollimation Shocks in the Core of 1803+784. *Astrophys. J.* **2013**, 772, 14. [CrossRef]
- 20. Zhang, H.; Li, X.; Giannios, D.; Guo, F. First-Principles Prediction of X-ray Polarization from Magnetic Reconnection in High-Frequency BL Lacertae Objects. *Astrophys. J.* **2021**, *912*, 129. [CrossRef]
- 21. Tavecchio, F. Probing Magnetic Fields and Acceleration Mechanisms in Blazar Jets with X-Ray Polarimetry. *Galaxies* **2021**, *9*, 37. [CrossRef]
- 22. Peirson, A.L.; Romani, R.W. The Polarization Behavior of Relativistic Synchrotron Jets. Astrophys. J. 2018, 864, 140. [CrossRef]
- 23. Marscher, A.P.; Jorstad, S.G.; D'Arcangelo, F.D.; Smith, P.S.; Williams, G.G.; Larionov, V.M.; Oh, H.; Olmstead, A.R.; Aller, M.F.; Aller, H.D.; et al. The Inner Jet of an Active Galactic Nucleus as Revealed by a Radio to Gamma-ray Outburst. *Nature* **2008**, 452, 966–969. [CrossRef] [PubMed]
- 24. Marscher, A.P.; Jorstad, S.G.; Larionov, V.M.; Aller, M.F.; Aller, H.D.; Lähteenmäki, A.; Agudo, I.; Smith, P.S.; Gurwell, M.; Hagen-Thorn, V.A.; et al. Probing the Inner Jet of the Quasar PKS 1510-089 with Multi-waveband Monitoring during Strong Gamma-ray Activity. *Astrophys. J. Lett.* **2010**, 710, L126–L131. [CrossRef]
- 25. Bodo, G.; Tavecchio, F.; Sironi, L. Kink-Driven Magnetic Reconnection in Relativistic Jets: Consequences for X-ray Polarimetry of BL Lacs. *Mon. Not. R. Astron. Soc.* **2021**, *501*, 2836–2847. [CrossRef]
- 26. Dong, L.; Zhang, H.; Giannios, D. Kink Instabilities in Relativistic Jets Can Drive Quasi-Periodic Radiation Signatures. *Mon. Not. R. Astron. Soc.* **2020**, 494, 1817–1825. [CrossRef]
- 27. Jorstad, S.G.; Marscher, A.P.; Raiteri, C.M.; Villata, M.; Weaver, Z.R.; Zhang, H.; Dong, L.; Gómez, J.L.; Perel, M.V.; Savchenko, S.S.; et al. Rapid Periodic Oscillations in the Relativistic Jet of BL Lacertae. *Nature* 2022, 609, 265–268. [CrossRef]
- 28. Williamson, K.E.; Jorstad, S.G.; Marscher, A.P.; Larionov, V.M.; Smith, P.S.; Agudo, I.; Arkharov, A.A.; Blinov, D.A.; Casadio, C.; Efimova, N.V.; et al. Comprehensive Monitoring of Gamma-ray Bright Blazars: Statistical Study of Optical, X-ray, and Gamma-ray Spectral Slopes. *Astrophys. J.* 2014, 789, 135. [CrossRef]
- 29. Weisskopf, M.C.; Soffitta, P.; Baldini, L.; Ramsey, B.D.; O'Dell, S.L.; Romani, R.W.; Matt, G.; Deininger, W.D.; Baumgartner, W.H.; Bellazzini, R.; et al. The Imaging X-Ray Polarimetry Explorer (IXPE): Pre-Launch. *J. Astron. Telesc. Instrum. Syst.* **2022**, *8*, 026002. [CrossRef]
- 30. DiGesu, L.; Donnarumma, I.; Tavecchio, F.; Agudo, I.; Barnounan, T.; Cibrario, N.; Di Lalla, N.; Di Marco, A.; Escudero, J.; Errando, M.; et al. The X-Ray Polarization View of Mrk 421 in an Average Flux State as Observed by the Imaging X-Ray Polarimetry Explorer. *Astrophys. J. Lett.* **2022**, *938*, L7. [CrossRef]
- 31. Liodakis, I.; Marscher, A.P.; Agudo, I.; Berdyugin, A.V.; Bernardos, M.I.; Bonnoli, G.; Borman, G.A.; Casadio, C.; Casanova, V.; Cavazzuti, E.; et al. Polarized Blazar X-Rays Imply Particle Acceleration in Shocks. *Nature* **2022**, *611*, *677*–*681*. [CrossRef]
- 32. Weaver, Z.R.; Jorstad, S.G.; Marscher, A.P.; Morozova, D.A.; Troitsky, I.S.; Agudo, I.; Gómez, J.L.; Lähteenmäki, A.; Tammi, J.; Tornikoski, M. Kinematics of Parsec-Scale Jets of Gamma-Ray Bright Blazars at 43 GHz during Ten Years of the VLBA-BU-BLAZAR Program. *Astrophys. J. Suppl.* 2022, 260, 12. [CrossRef]
- 33. Blazar Research at Boston University: 1959+650. Available online: https://www.bu.edu/blazars/VLBA\_GLAST/1959.html (accessed on 30 September 2022).
- 34. Marscher, A.P.; Gear, W.K. Models for High-Frequency Radio Outbursts in Extragalactic Sources with Application to the Early 1983 Millimeter to Infrared Flare of 3C273. *Astrophys. J.* 1985, 298, 114–127. [CrossRef]
- 35. Weaver, Z.R.; Williamson, K.E.; Jorstad, S.G.; Marscher, A.P.; Larionov, V.M.; Raiteri, C.M.; Villata, M.; Acosta-Pulido, J.A.; Bachev, R.; Baida, G.V.; et al. Multi-wavelength Variability of BL Lacertae Measured with High Time Resolution. *Astrophys. J.* **2020**, *900*, 137. [CrossRef]
- 36. Albert, A.; Alfaro, R.; Alvarez, C.; Camacho, J.A.; Arteaga-Velázquez, J.C.; Arunbabu, K.P.; Rojas, D.A.; Solares, H.A.; Baghmanyan, V.; Belmont-Moreno, E.; et al. Long-term Spectra of the Blazars Mrk 421 and Mrk 501 at TeV Energies Seen by HAWC. *Astrophys. J.* 2022, 929, 125. [CrossRef]
- 37. Abdo, A.A.; Ackermann, M.; Agudo, I.; Ajello, M.; Aller, H.D.; Aller, M.F.; Angelakis, E.; Arkharov, A.A.; Axelsson, M.; Bach, U.; et al. The Spectral Energy Distribution of Fermi Bright Blazars. *Astrophys. J.* **2010**, *716*, 30–70. [CrossRef]
- 38. Blandford, R.D.; Znajek, R. Electromagnetic extraction of energy from Kerr black holes. *Mon. Not. R. Astron. Soc.* **1977**, 179, 433–456. [CrossRef]
- 39. McKinney, J.C.; Narayan, R. Disc-jet Coupling in Black Hole Accretion Systems I. General Relativistic Magnetohydrodynamical Models. *Mon. Not. R. Astron. Soc.* **2007**, 375, 513–530. [CrossRef]
- 40. Tchekhovskoy, A.; Narayan, R.; McKinney, J.C. Efficient Generation of Jets from Magnetically Arrested Accretion on a Rapidly Spinning Black Hole. *Mon. Not. R. Astron. Soc.* **2011**, *418*, L79–L83. [CrossRef]
- 41. Meier, D.L.; Koide, S.; Uchida, Y. Magnetohydrodynamic Production of Relativistic Jets. Science 2001, 291, 84–92. [CrossRef]
- 42. Vlahakis, N. Disk-Jet Connection. In *Blazar Variability Workshop II: Entering the GLAST Era*; Miller, H.R., Marshall, K., Webb, J.R., Aller, M.F., Eds.; Astronomical Society of the Pacific: San Francisco, CA, USA, 2006; Volume 350, pp. 169–177.

Universe **2022**, 8, 644 10 of 10

43. Zamaninasab, M.; Clausen-Brown, E.; Savolainen, T.; Tchekhovskoy, A. Dynamically Important Magnetic Fields near Accreting Supermassive Black Holes. *Nature* **2014**, *510*, 126–128. [CrossRef]

- 44. Nalewajko, K.; Begelman, M.C. The Effect of Poloidal Velocity Shear on the Local Development of Current-Driven Instabilities. *Mon. Not. R. Astron. Soc.* **2012**, 427, 2480–2486. [CrossRef]
- 45. Tavecchio, F.; Landoni, M.; Sironi, L.; Coppi, P. Probing Dissipation Mechanisms in BL Lac Jets through X-ray Polarimetry. *Mon. Not. R. Astron. Soc.* **2018**, *480*, 2872–2880. [CrossRef]
- 46. Burn, B.J. On the Depolarization of Discrete Radio Sources by Faraday Dispersion. *Mon. Not. R. Astron. Soc.* **1966**, *133*, 67–83. [CrossRef]
- 47. Jones, T.W. Polarization as a Probe of Magnetic Field and Plasma Properties of Compact Radio Sources—Simulation of Relativistic Jets. *Astrophys. J.* **1988**, 332, 678–695. [CrossRef]
- 48. Webb, J.R.; Arroyave, V.; Laurence, D.; Revesz, S.; Bhatta, G.; Hollingsworth, H.; Dahlla, S.; Howard, E.; Cioffi, M. The Nature of Micro-Variability in Blazars. *Galaxies* **2021**, *9*, 114. [CrossRef]
- 49. Smith, P.S.; Montiel, E.; Rightley, S.; Turner, J.; Schmidt, G.D.; Jannuzi, B.T. Coordinated Fermi/Optical Monitoring of Blazars and the Great 2009 September Gamma-Ray Flare of 3C 454.3. In Proceedings of the 2009 Fermi Symposium, eConf Proceedings C091122, Washington, DC, USA, 2–5 November 2009.
- 50. Zhang, H.; Fang, K.; Li, H.; Giannios, D.; Böttcher, M.; Buson, S. Probing the Emission Mechanism and Magnetic Field of Neutrino Blazars with Multiwavelength Polarization Signatures. *Astrophys. J.* **2019**, *876*, 109. [CrossRef]
- 51. Peirson, A.L.; Romani, R.W. The Polarization Behavior of Relativistic Synchrotron Self-Compton Jets. *Astrophys. J.* **2019**, *856*, 76. [CrossRef]